DEVELOPING INFRARED (IR) TRANSPARENT CONDUCTIVE ELECTRODE TECHNOLOGY FOR MULTI-FUNCTIONAL INFRARED (IR) SENSING

Final Report

Reporting Period: February 15, 2008— February 28, 2011

Contract No.: FA9550-08-1-0070

Dr. Xuejun Lu
Title: Associate professor
Email: Xuejun_Lu@uml.edu
Phone: 978-934-3359
Fax: 978-934-3027

Report to:

Dr. Kitt C Reinhardt

AFOSR

875 North Randolph Street

Arlington, VA 22203

REPORT DOCUMENTATION PAGE

Form Approved OMB No. 0704-0188

1. REPORT DATE *(DD-MM-YYYY)*	2. REPORT TYPE	3. DATES COVERED *(From - To)*
13-07-2011	Final report	02/15/2008–02/28/2011

4. TITLE AND SUBTITLE
DEVELOPING INFRARED (IR) TRANSPARENT CONDUCTIVE ELECTRODE TECHNOLOGY FOR MULTI-FUNCTIONAL INFRARED (IR) SENSING

5a. CONTRACT NUMBER
FA9550-08-1-0070

5b. GRANT NUMBER
same

5c. PROGRAM ELEMENT NUMBER

6. AUTHOR(S)
Xuejun Lu

5d. PROJECT NUMBER

5e. TASK NUMBER

5f. WORK UNIT NUMBER

7. PERFORMING ORGANIZATION NAME(S) AND ADDRESS(ES)
University of Massachusetts Lowell
1 University Ave.
Lowell, MA 01854
Tel: 978-934-3359
Fax: 978-934-3027

8. PERFORMING ORGANIZATION REPORT

9. SPONSORING / MONITORING AGENCY NAME(S) AND ADDRESS(ES)
Kitt C Reinhardt
AFOSR
875 North Randolph Street
Arlington, VA 22203

10. SPONSOR/MONITOR'S ACRONYM(S)

11. SPONSOR/MONITOR'S REPORT NUMBER(S)

12. DISTRIBUTION / AVAILABILITY STATEMENT

13. SUPPLEMENTARY NOTES

14. ABSTRACT

Transparent conductive electrode technology has long been desired in a great variety of applications, such as light-emitting diode (LED), solar cells, transparent smart skins, invisible electronics and antennas, and embedded sensing and imaging. Current state-of-the-art transparent conductive electrode technology is based on indium tin oxide (ITO). However, ITO is high transparent only in the visible region. In MIR/LWIR spectrum region, the transmission of the ITO electrode is poor. (Our recent results indicate that high-quality Carbon nanotubes (CNT) thin-film also has low sheet resistance and high transmission over a broadband spectral region from visible (400 nm) through longwave infrared (~12 μm). Such broadband transparent and conductive properties together with its excellent mechanical flexibility make the CNT film a promising candidate for transparent conductive electrodes that can be used for broad-area of applications, including light-emitting diode (LED), solar cells, transparent smart skins, transparent electronics and antennas for embedded sensing and imaging. In this AFOSR program, the properties of the CNT-based transparent conductive electrode film have been investigated, including work function, surface contact resistance and interfacial stability. The reliability the CNT transparent electrode film is also evaluated.

15. SUBJECT TERMS
Carbon nanotube (CNT), infrared transparent conductive film, flexible thin-film transistors

16. SECURITY CLASSIFICATION OF:			17. LIMITATION OF ABSTRACT	18. NUMBER OF PAGES	19a. NAME OF RESPONSIBLE PERSON
a. REPORT	b. ABSTRACT	c. THIS PAGE		25	Xuejun Lu
					19b. TELEPHONE NUMBER *(include area code)* 978-934-3359

Standard Form 298 (Rev. 8-98)
Prescribed by ANSI Std. Z39.18

TABLE OF CONTENTS

List of figures

LIST OF TABLES

1. APPLICATIONS AND BACKGROUND

Transparent conductive electrode technology has long been desired in a great variety of applications, such as light-emitting diode (LED), solar cells, transparent smart skins, invisible electronics and antennas, and embedded sensing and imaging. Particularly, transparent electrodes in IR spectrum region can be integrated with IR sensors and focal plane array (FPA) to provide multi-functionalities such as transparent electrical interconnects for on-chip signal processing and tunable filters for pixel-wise embedded spectral analysis. Such integrated functionalities would not only enhance the pixel-level sensing and processing capabilities (smart pixel), but also greatly reduce the communication traffic loads between the image sensors and the subsequent image processing electronics. This would enable high-throughput IR sensing and target detection with enhanced characterization and discrimination capabilities.

The state-of-the-art transparent conductive electrode technology is based on indium tin oxide (ITO) [1-4]. While the ITO based transparent conductive electrodes are extensively used in LCD display, solar cells and LEDs, there are a few issues related to the ITO technology. One is that ITO has poor mechanical flexibility and is brittle. The other is that high quality ITO films can only be obtained at substrate temperature over 300 °C. Depositing ITO films at low substrate temperatures (below 300 °C) results in opaque films with high sheet resistance (> 500 Ohms/sq) [2]. The poor mechanical flexibility and high substrate temperature requirement seriously limit its applications in flexible devices, such as flexible display, organic solar cell, and smart skin technology. In addition, ITO is transparent only at visible region. It is highly absorptive at middle infrared (MIR, 3-5μm) and longwave infrared (LWIR, 8-12μm) regions, and are thus not suitable for applications in MIR and LWIR spectral region.

Carbon nanotubes (CNT) [5-9], as a new material with exceptional aspect ratio and great mechanical flexibility, have shown excellent thermal conductivity and extremely high field-effect mobility of over 100,000 cm^2/Vs [6-9]. Carbon nanotubes (CNT), a novel material with great mechanical flexibility, have shown excellent thermal conductivity and extremely high field-effect mobility. Our recent results indicate that high-quality CNT thin-film also has low sheet resistance and high transmission over a broadband spectral region from visible (400 nm) through longwave infrared (~12 μm). Such broadband transparent and conductive properties together with its excellent mechanical flexibility make the CNT film a promising candidate for transparent conductive electrodes that can be used for broad-area of applications, including light-emitting diode (LED), solar cells, transparent smart skins, transparent electronics and antennas for embedded sensing and imaging.

Despite the promising characteristics of the CNT transparent conductive film, electrical parameters of the CNT film, such as work function and contact resistance on different semiconductor surfaces such as Si, GaAs and InP, are not available. Such parameters are critical in achieving good Ohmic contact on these semiconductor surfaces. Also highly desired is to evaluate the reliabilities of the CNT film and develop reliability enhancement techniques, especially for space applications. The goal of this research is to specifically address these issues. The objectives of the AFOSR research program proposed research are to:

(1) Obtain electrical parameters of the CNT film, including work function and contact resistance of the CNT film on different semiconductors.

(2) Develop effective doping and transmission spectrum window tuning and engineering techniques.

(3) Evaluate reliability of the CNT film and develop reliability enhancement techniques.

In the AFOSR research, we have performed the following three research tasks, plus a report task:

- Task 1: Obtain detailed electrical and spectrum parameters of the CNT film
- Task 2: Develop effective doping and transmission spectrum window tuning and engineering techniques
- Task 3: Evaluate reliability of the CNT film and develop reliability enhancement techniques
- Task 4: Reporting

2. DETILED RESEARCH REPORT

2.1 Took SEM image and measured the IR-transmission spectrum of the CNT film

Fig. 1 (a) shows the SEM image and the IR-transmission spectrum of the CNT film (pink curve), respectively. The IR-transmission spectrum ITO film is also shown in Fig. 1(b) (blue curve) for comparison. The CNT film shows a high transmission of > 95% from 7μm to 10μm and from 11μm to 12μm and a low sheet resistance of 200Ω/sq. Our measurement results are consistent with published results [10-11]. Such good transmission in IR region and low resistance provide an unprecedented opportunity to achieve IR transparent conductive electrode.

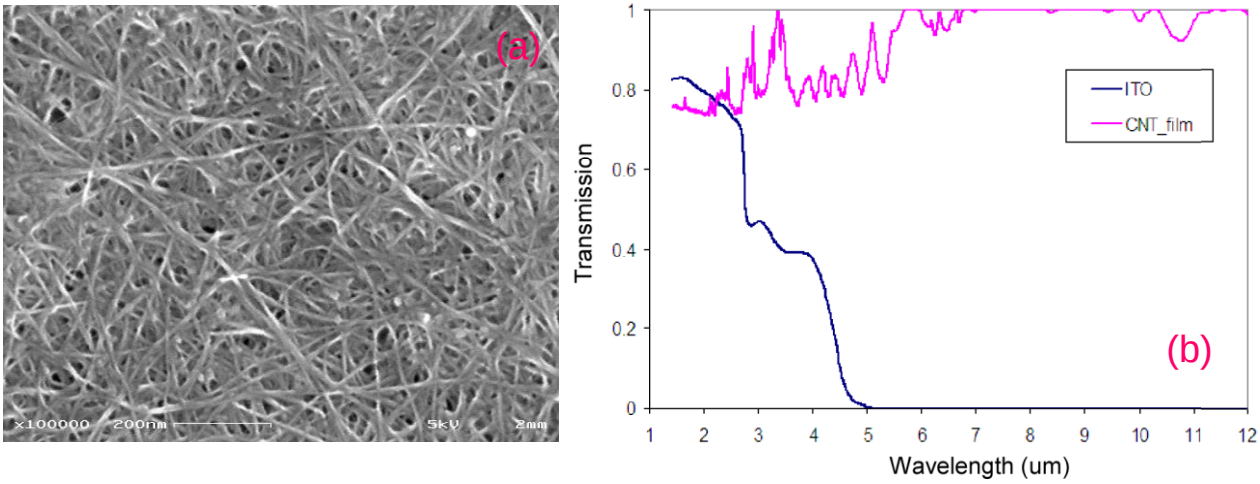

Figure 1. (a) SEM image and (b), IR-transmission spectrum of the CNT film (pink curve), and transmission spectrum of an ITO film (blue curve). The CNT film shows a high transmission of > 95% from 7μm to 10μm and from 11μm to 12μm and a low sheet resistance of 200Ω/sq.

To compare the conductivity of the CNT film with that of an ITO film, three points on the ITO glass were randomly chosen and the resistances between these points were measured to be R_{AB} = 0.32k Ω, and R_{BC} = 0.30 k Ω, respectively. This is shown in Fig. 2(a). Then these points are isolated by etching away the ITO within the 0.5 inch-wide stripes between theses points, as shown in Fig. 3(b). The PI then coated the 0.5 inch-wide stripes with CNT films (Fig. 2(b)) and re-measured the resistances between these points to be R_{AB} = 1.3k Ω, and R_{BC} = 1.1 k Ω, respectively. The transmissions of the CNT films were confirmed to be over 95% over the visible spectrum by a PerkinElmer UV-VIS absorption spectrometer. This experiment demonstrated that the CNT film is promising for transparent conductive electrode.

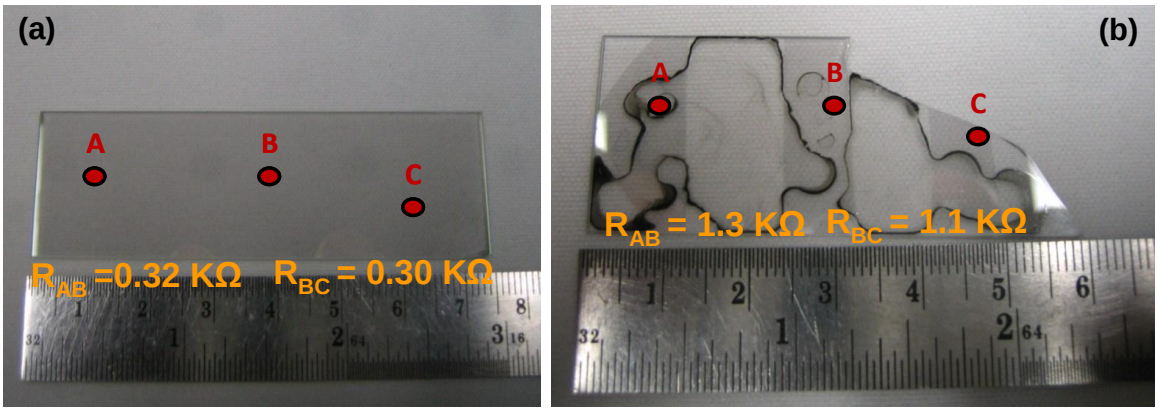

Figure 2. (a) Resistances between randomly chosen points on an ITO glass; (b) Etching away ITO stripes, recoated with CNT films, and re-measured the resistances between the pre-chosen points.

2.2 Determined the work function the CNT film

In this research period, we have performed research to determined the work function of CNT film to. The schematic of the proposed measurement setup is shown in Fig. 3(a).

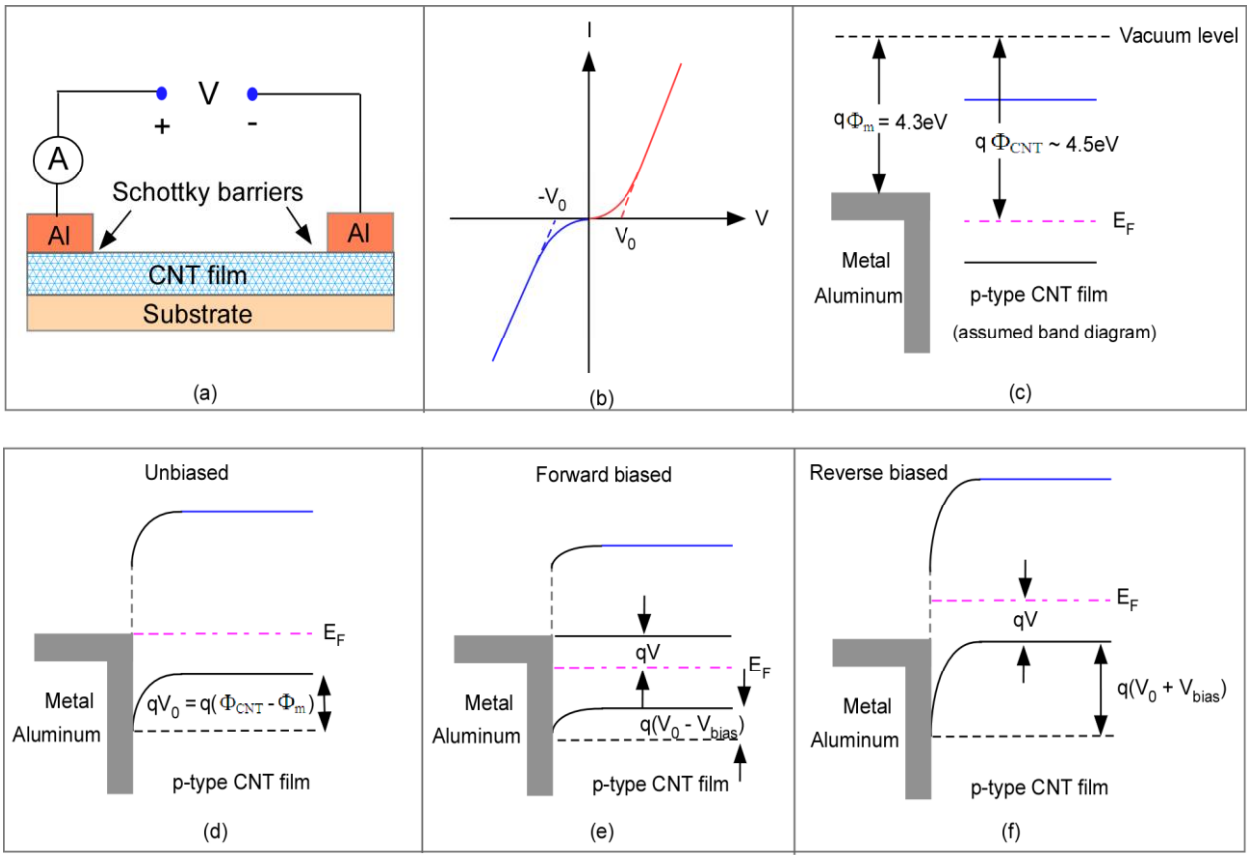

Figure 3, (a) Schematic setup for the CNT work function measurement; (b) Expected I-V curve of the CNT-metal Schottky barrier; (c), Band diagrams of Aluminum and the p-type doped CNT film; (d) – (f), The band diagrams of the Al-CNT film Schottky barrier at zero-bias, forward and reverse bias, respectively.

The setup is to measure the I-V curve of the Schottky barrier formed between aluminum(Al) with known work function Φ_s = 4.3eV and the CNT film. From the I-V curve (Fig. 3(b)), we measured the threshold voltage of the Schottky barrier V_0, which is related to the work function of the metal and that of the CNT film by:

$$qV_0 = q(\Phi_{CNT} - \Phi_m), \quad (1)$$

The work function of the CNT film can thus be obtained by:

$$\Phi_{CNT} = V_0 + \Phi_m, \quad (2)$$

The I-V characteristic of the CNT-metal Schottky diode is shown in Fig. 4. The turn-on voltage of the CNT-metal Schottky diode is determined to be 0.5V. The Fermi level of the CNT film is thus determined to be 4.8eV, which is 0.3eV high than the single CNT. This high Fermi-level is possibly due to the electro-withdrawing function groups that make it harder to take an electron away from the CNF film and thus increase the Fermi level of the CNT film.

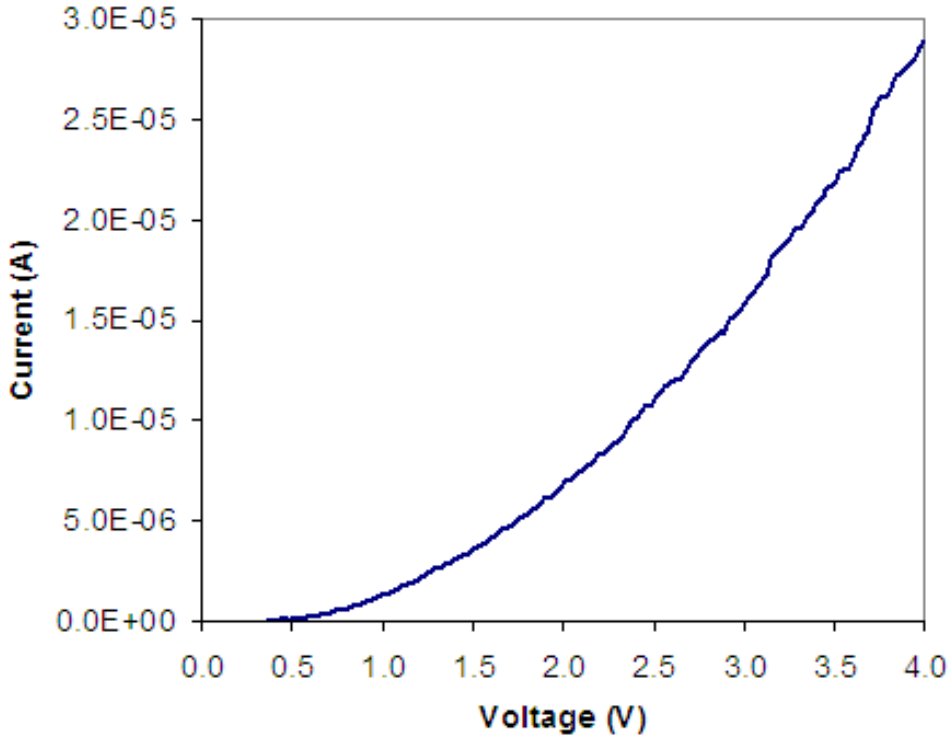

Figure 4. I-V Characteristics of the CNT-metal Schottky barrier. The CNT-metal Schottky diode turns on at ~ 0.5V. The Fermi-level of the CNF film is determined to be ~ 4.8eV.

2.3 Determined the contact resistance and the mobility of the CNT film

Fig. 5 shows the I-V curve of CNT film. The sample has four Al blocks, the width between block 1 and 2 is about 3mm, between 2 and 3 is about 9mm, between 3 and 4 is about 3mm.

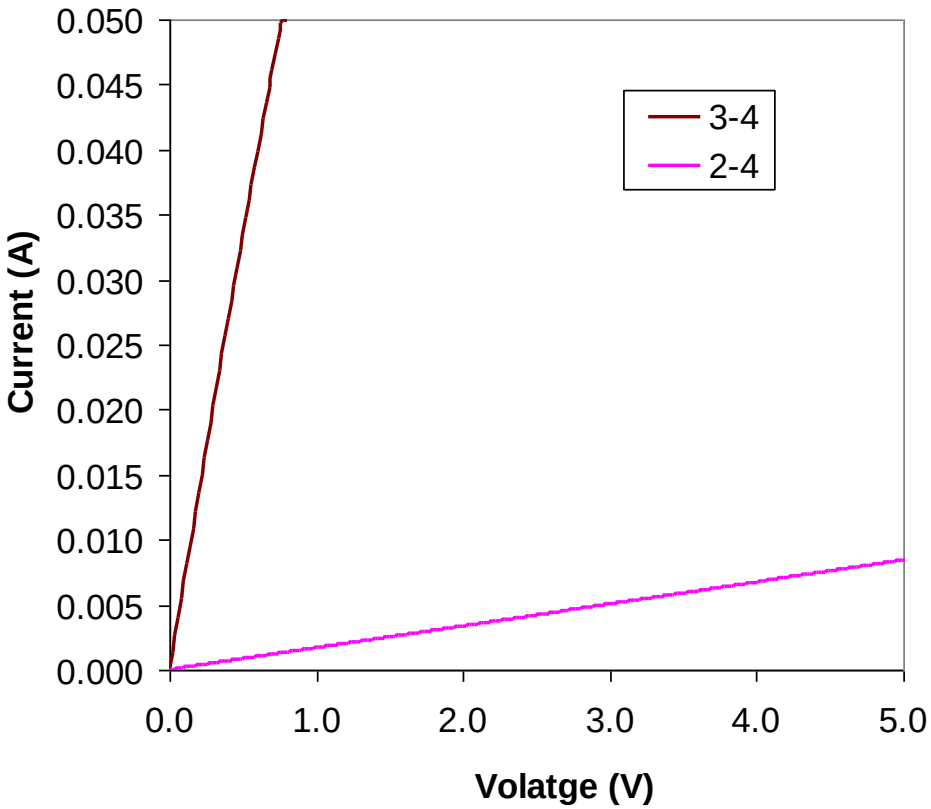

Figure 5, I-V curve of CNT film.

From Fig. 5, the resistance between 2 and 4 is determined to be 596Ω, and the resistance between 3 and 4 is determined to be 15Ω. The resistance between 2-4 R_{24} can be written as:

$$R_{2-4} = 4R_{cont} + R_{2-3} + R_{3-4}, \quad (3)$$

where, R_{34} is the resistance between 3 and 4, and R_{cont} is the contact resistance, which is therefore determined to be 134 Ω.

The current density can be written as:

$$J = \sigma E = e\mu nE, \quad (4)$$

where, n is the density of the carriers, e is the charge of an electron, and μ is the mobility of the carriers, and E is the electric field. Assuming the carrier density is 1x1018cm-3, the mobility is calculated to be 43,000 cm^2/Vs. The high mobility indicates that the CNT film is a good conductor.

2.4 Determined the transmission of the CNT film and its sheet resistance

We investigated the CNTs in DI water solution. Fig. 6 shows the transmission spectrum of the CNT films. A transmission of over 40% were obtained. The sheet resistances were measured using a four point probe to be R_{sheet} = 146 Ω. Fig. 7 shows the transmission of CNT film at 550 nm as a function of sheet resistance. An around 80% transmission at 550nm can be obtained at a sheet resistance value of ~ R_{sheet} = 15 k Ω.

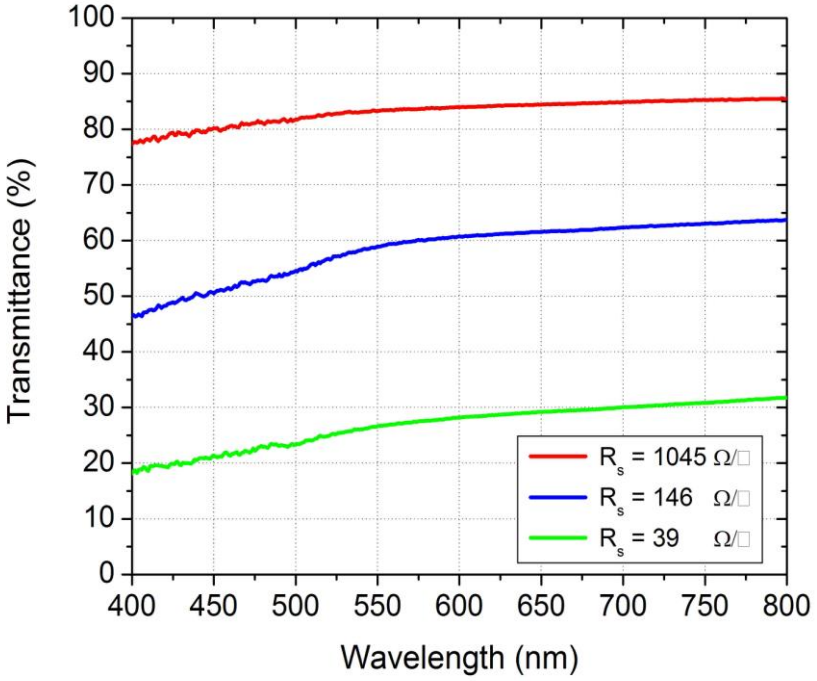

Figure 6. Transmission spectrum of the CNT films. A transmission of over 40% were obtained at a sheet resistance value of 146 Ω. .

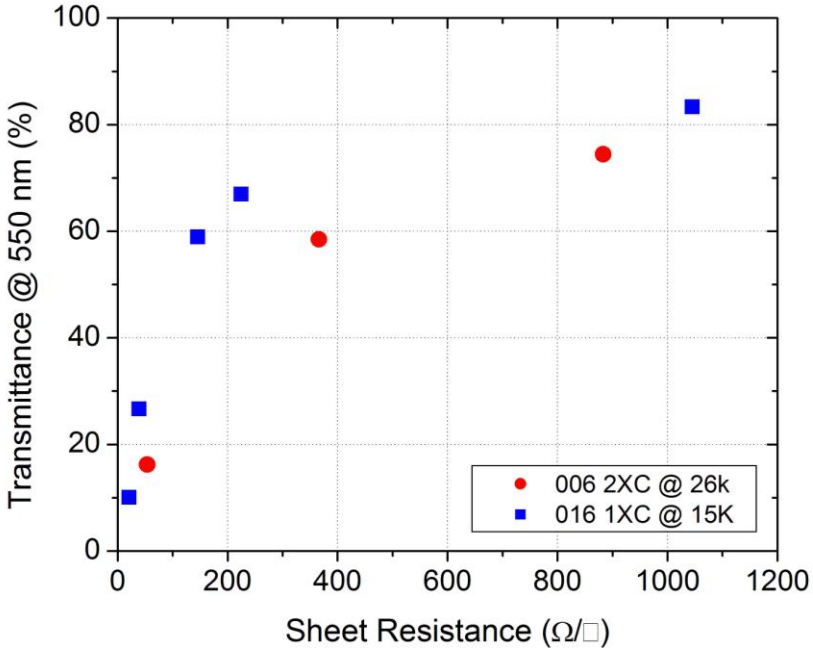

Figure 7, Transmission of CNT film at 550nm as a function of sheet resistance.

2.5 Investigated the doping of different chemical function groups and their effects on the work function of CNTs

We have investigated the doping of different chemical function groups and their effects on the work function of CNTs by measuring the I-V characteristics of four different CNT solutions with chemical function groups as listed in Table 1.

Table 1, CNT solutions under test

CNT No.	Description of the CNT	Symbol
1	Dispersed SWNTs 90wt% 1-2nm CNT Concentration: 3g/L Surfactant: PVP Solvent: DI water	CNT
3	Dispersed Short SWNTs 90wt% 1-2nm OH CNT Concentration: 3g/L Surfactant: PVP Solvent: Ethanol	CNT-OH
4	Dispersed SWNTs 90wt% 1-2nm COOH CNT Concentration: 3g/L Surfactant: PVP Solvent: DI water	CNT-COOH

Fig. 8 shows the schematic setup of the I-V characteristic measurement.

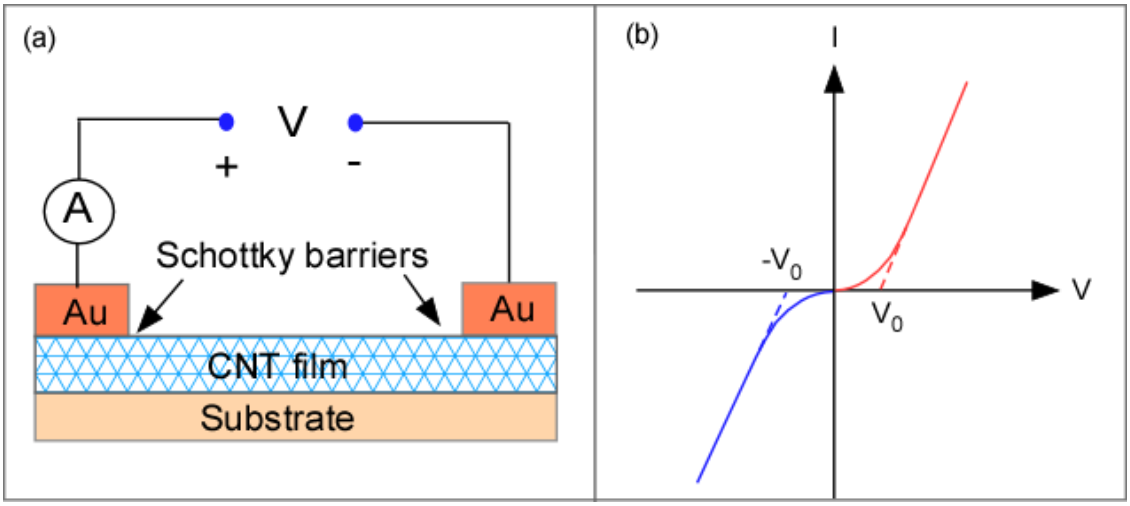

Figure 8, Schematic view of the I-V characteristics measurement.

By measuring the turn-on voltage of the I-V curves, the Schottky barrier between the metal and the CNT can be obtained. The simplified energy band diagrams of the CNT and metal interface before and after the contact are shown in Fig. 8 (a) and (b), respectively.

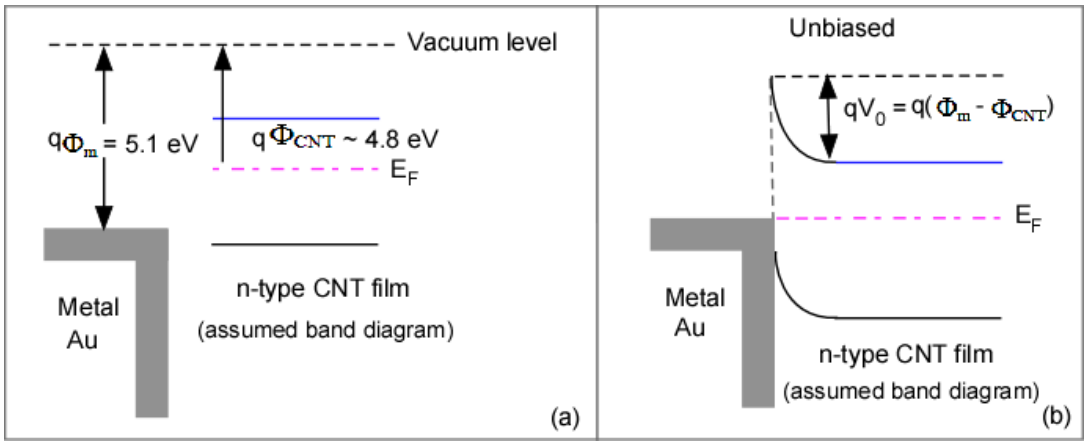

Figure 9. Simplified energy band diagrams of the CNT and metal interface: (a) before contact; (b) after contact. A barrier V0 is formed between the interface.

The measured I-V curves for CNT and CNT-OH are shown in Fig. 10. The inset shows the band diagram, respectively.

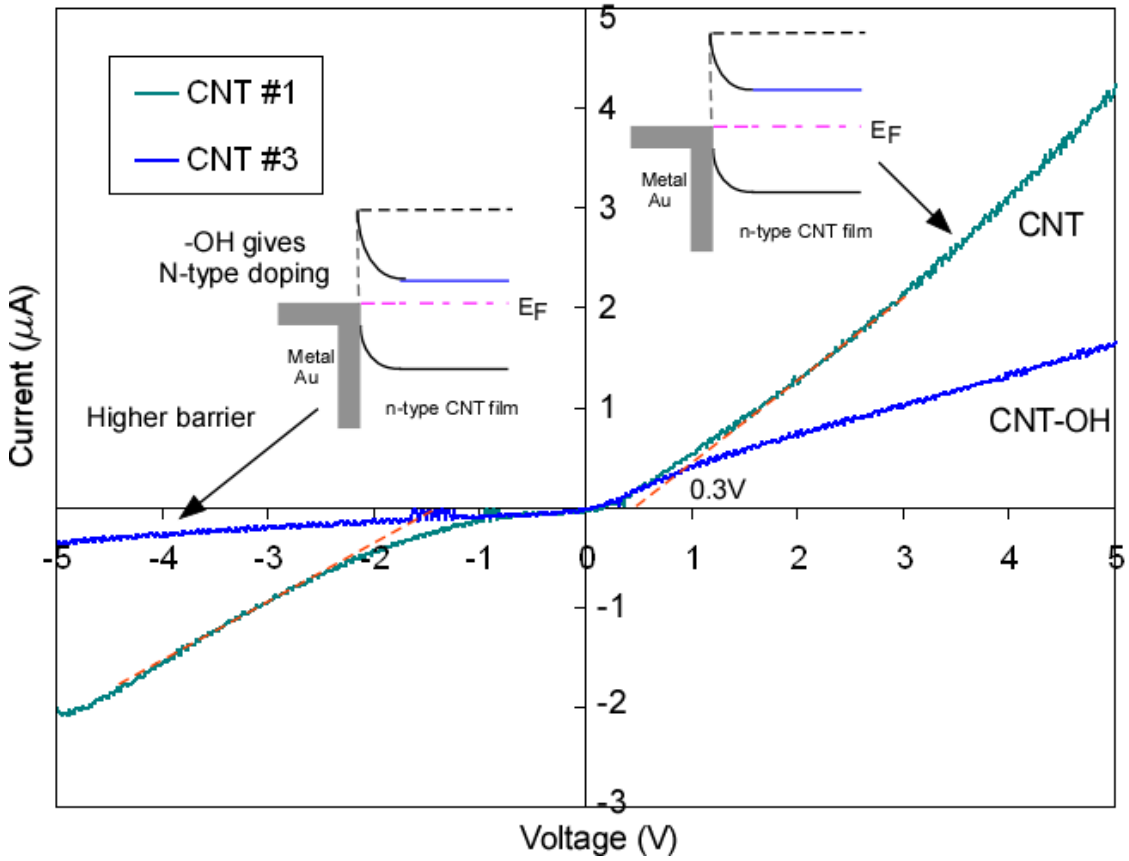

Figure 10, Measured I-V curves for CNT and CNT-OH. The inset shows the band diagram**.**

The CNT-OH shows a lower current at the same bias voltage as compared with the CNT. This indicates that CNT-OH has a higher barrier at the Au interface. This indicates that the –OH chemical function gives N-type doping. This consists with the electron-donation

property of the –OH chemical function group. Table 2 shows different chemical function groups for electron-withdrawing and electron-donating.

Table 2, Electron-withdrawing and electron-donating chemical function groups

Electron-withdrawing function groups	**Electron-donating function groups**
-COOR, -COOH, -COR, -CHO, -NO_2, -CN -F, -Cl, -BR, -I, -CF_3 (where, R represents the group -CH_3)	-OH, -NH_2, -NR_2, -SH, -CR_3, -OR (where, R represents the group -CH_3)

From Table 2, the –COOH function group is an electron-withdrawing chemical function group. It is predicated that the –COOH function would move the Femi-level down and thus reduce the barrier between the metal and CNT interface. This is actually confirmed by our experimental results. Fig. 11 shows the I-V characteristic of the –COOH functionalized CNT film.

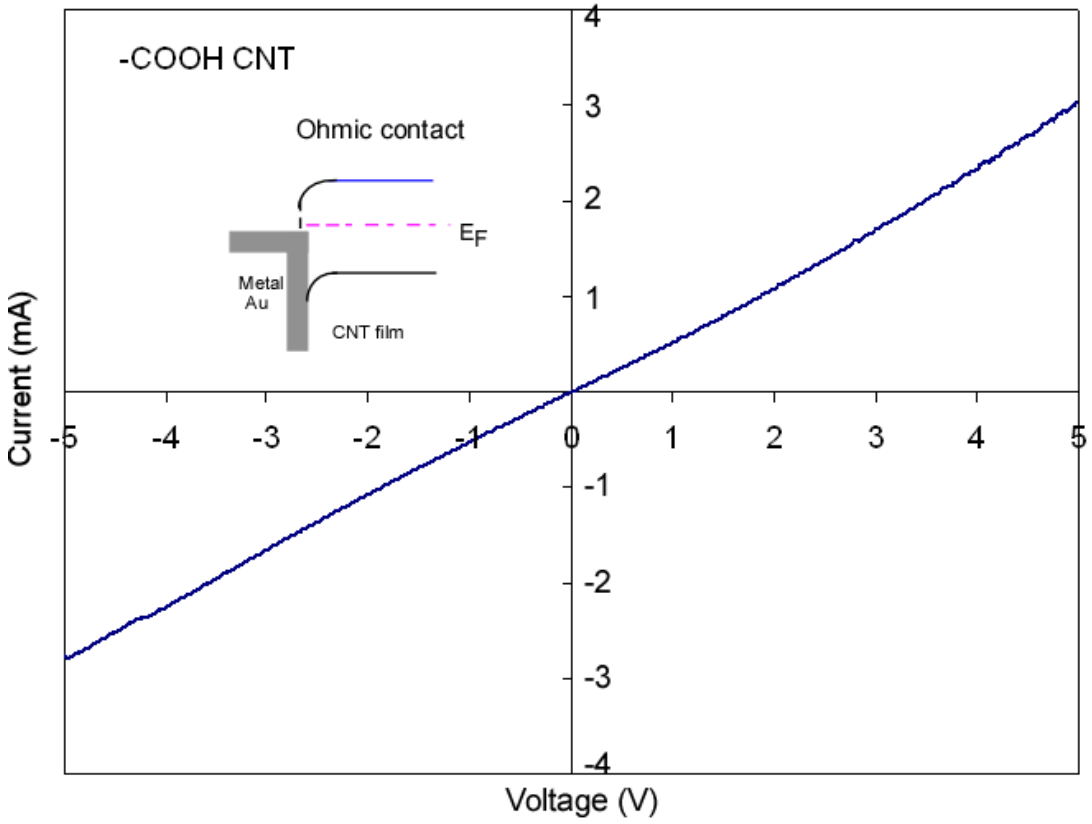

Figure 11, Measured I-V curves for CNT-COOH. The inset shows the band diagram**.**

The current is in the mA region. This is much larger that the currents of the CNT and the CNT-OH, which are both in the µA range. In addition, due to the electron-withdraw effect, the Fermi level is moved down and thus make the contact between the metal and the CNT become Ohmic contact.

This indicates that by functionalize the CNT with electron-donation or withdrawing chemical function groups, effective Fermi-level tuning can be achieved. Such Femi-level tuning can be used to change the barrier of the CNT and metal interface and make it either Ohmic contact or Schottky barrier.

2.6 Measured the CNT performance under different chemicals

We investigated the CNT film under the pressure of different chemicals. Fig. 12 shows current conduction of the CNT film in a small chamber with Alcohol (CH_3CH_2-OH) at different time intervals after it is put into the Alcohol chamber. From Fig. 12, one can see that at the beginning, the conductivity jump to a high level (the green curve, 1min). After that, we test the I-V curve every 1minute. From the following 8 minutes, the conductivity drop down gradually, but still higher than without Alcohol. This indicates that the Alcohol functions as an effective n-doping and increases the conductivity of the CNT film.

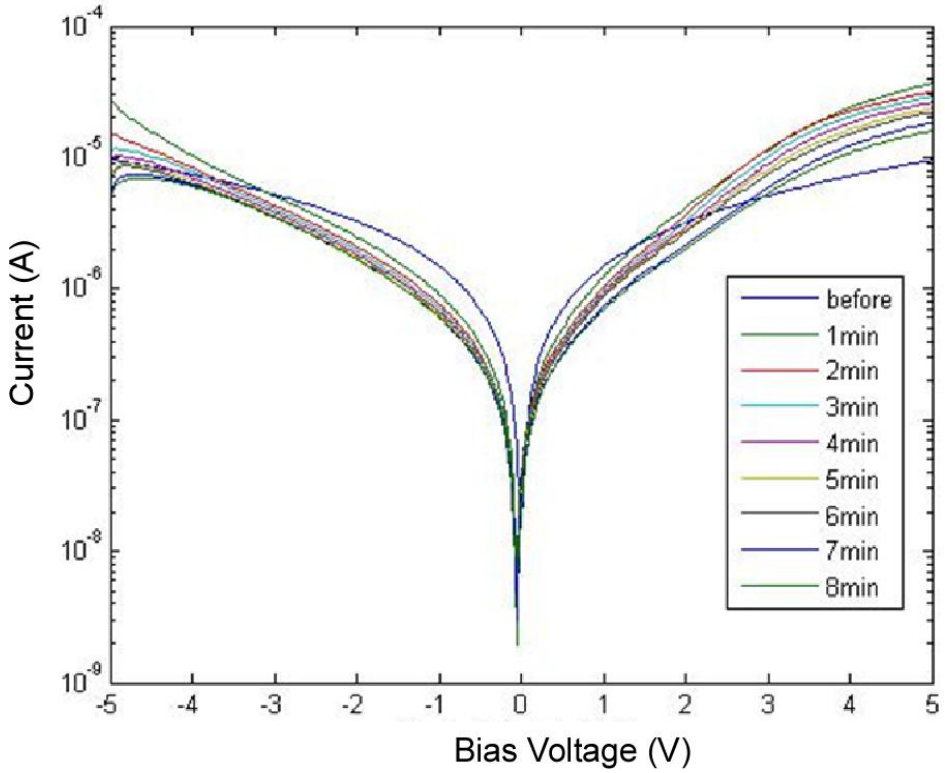

Figure 12, Current conduction of the CNT film in a small chamber with Alcohol (CH_3CH_2-OH) at different time intervals after the CNT film is put into the Alcohol chamber.

To check whether the conductivity of the CNT film can be restored to the original values, we, take out the CNT film from the chamber. We test the I-V curves after the Alcohol is gradually evaporated. Fig. 13 shows the I-V curves at different time intervals after the CNT film is taken out of the Alcohol chamber. From Fig. 13, the solid blue line stands for before we put the sensor into the chamber, the solid green, red and aqua lines are the status inside the chamber, while the following three is status outside the chamber. We can see that after take out from the chamber, the conductivity drop back, even lower than without the Alcohol, which indicate that the Alcohol may dilute the CNT solution, which directly lower the CNT density.

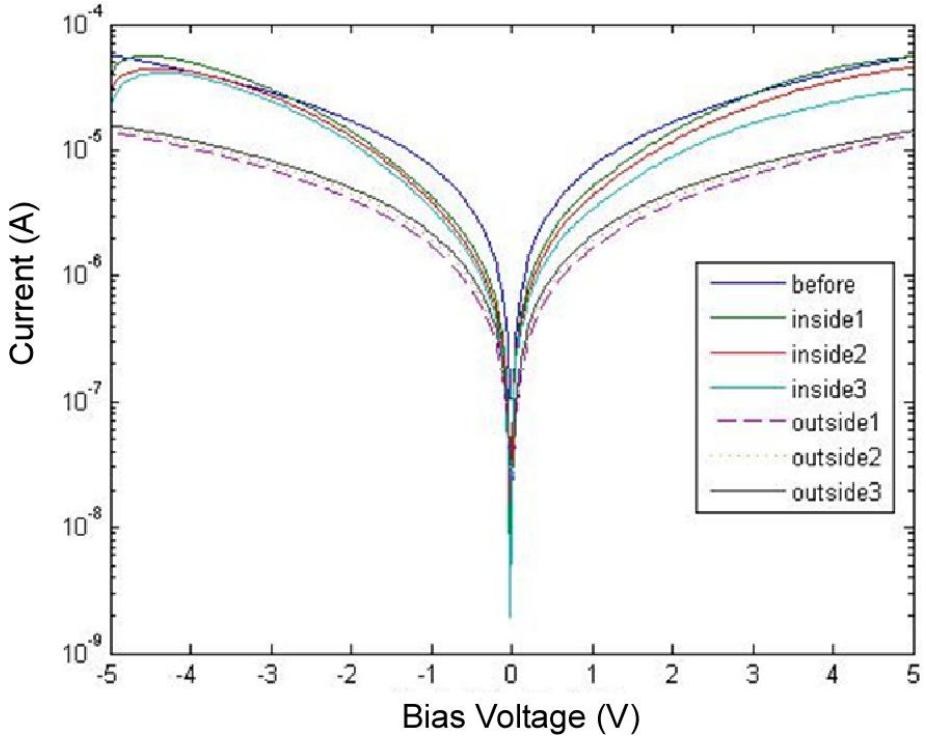

Figure 13, I-V curves at different time intervals after the CNT film is taken out of the Alcohol chamber.

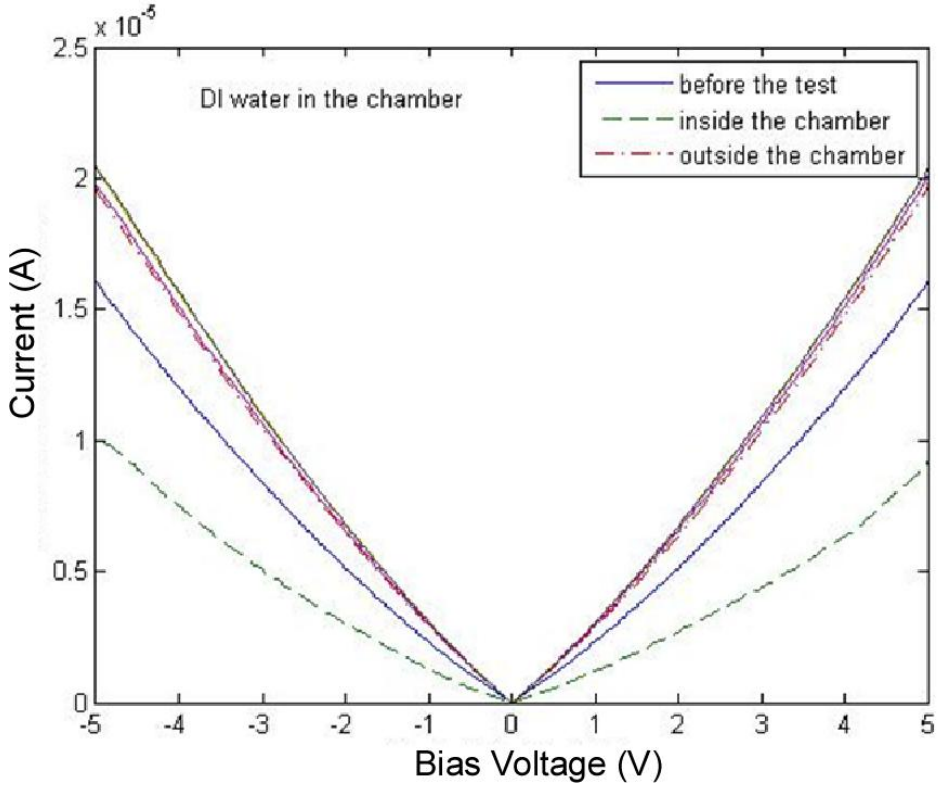

Figure 14, I-V curves before the CNT film is put into the water chamber and after it is taken out of the water chamber.

We also tested the CNT film under the pressure of water (H_2O). Fig. 14 shows the I-V curves before the CNT film is put into the water chamber and after it is taken out of the water chamber. From Fig. 14, one can see that the conductivity of the CNT film is low when it is inside the water chamber. After it is taken out of the water chamber, the conductivity goes up. This indicates that H_2O will not function as an effective doping for the CNT film and the H_2O dilutes the CNT and thus reduces the conductivity of the CNT film. Since the H_2O molecules are small, the conductivity restores when the H_2O molecules are removed from the CNT film.

2.7 Measured the CNT performance under different temperatures

We also tested the CNT film under the pressure of different temperatures. Fig. 15 shows the conductivity of the CNT film under different temperatures varying from room temperature 20 °C to 100 °C. The conductivity increases slightly with the sample temperature. This show the temperature stability of the CNT film.

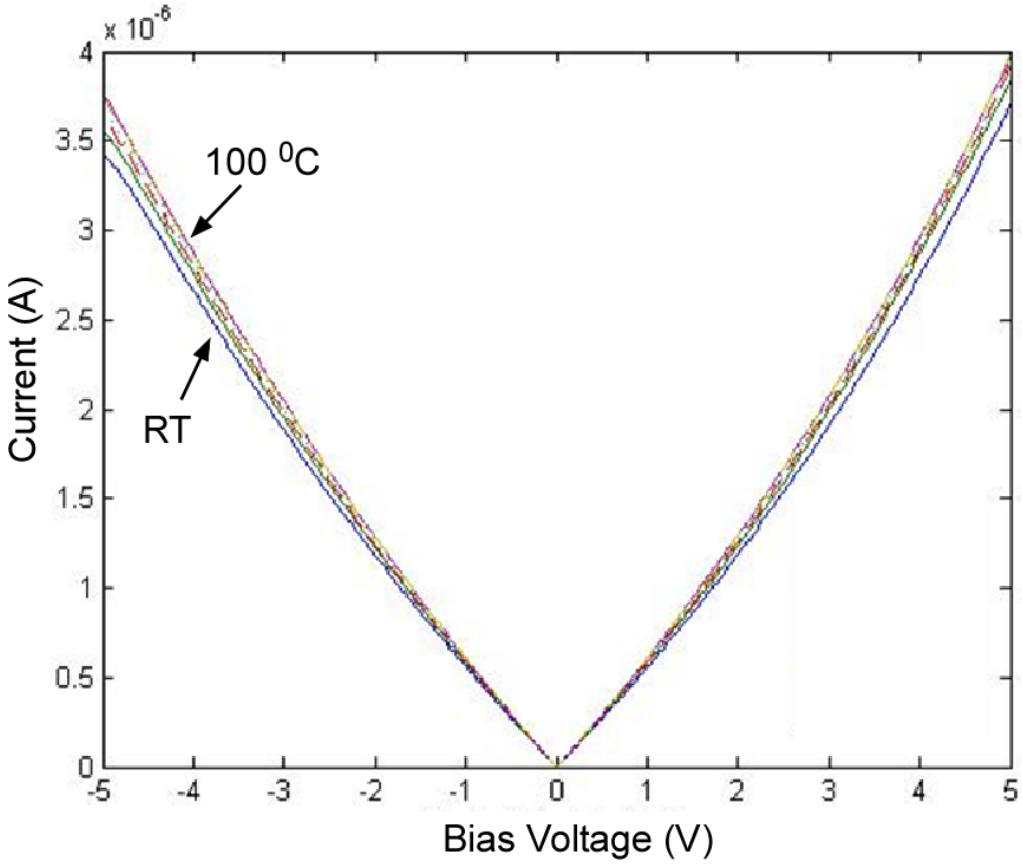

Figure 15, I-V curves of the CNT film under different temperatures varying from room temperature 20 °C to 100 °C.

2.8 Designed a MEMS based comb filter with integrated LWIR photodetector

Fig. 16 shows the schematic structure of the MEMS-based hyper-spectral QDIP. By tuning the bias of the transparent electrode coated on the membrane, the cavity length and corresponding passband of the filter can be changed accordingly. The electrode on the filter membrane is a new transparent conductive CNT thin-film network. Since the electrode is

transparent, low optical loss hyper-spectral IR sensing and imaging can be achieved. Such MEMS-based hyper-spectral QDIP would also enable quick spectral scan of IR characteristics of chemical and biological materials.

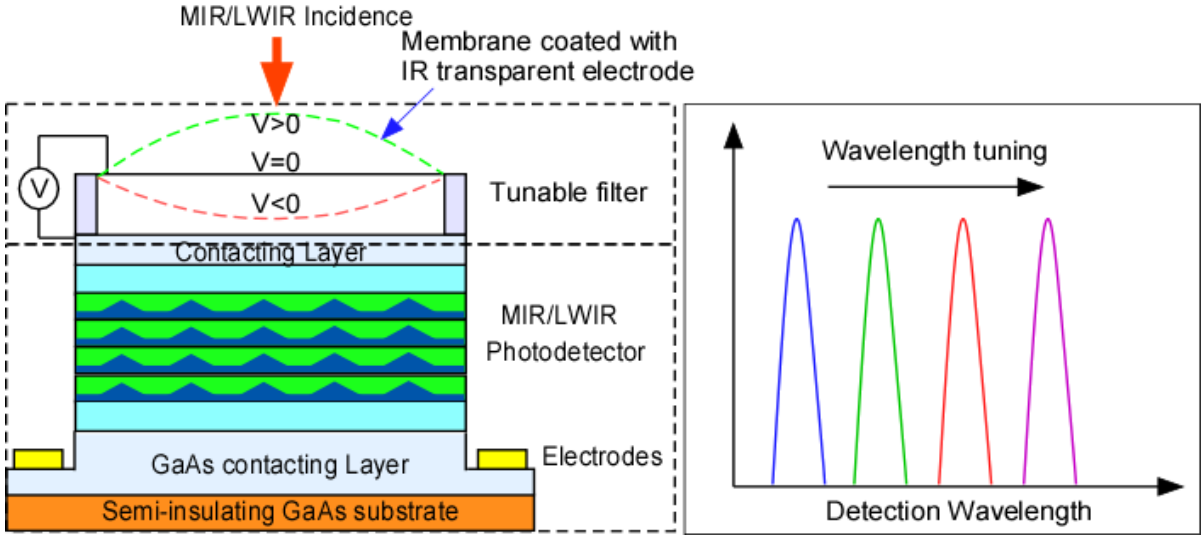

Figure 16, Schematic structure of the hyper-spectral IR Photodetector with integrated tunable filter.

The free spectral range (FSR) of the cavity, can be written as:

$$FSR = \frac{\lambda^2}{2nL}, \tag{5}$$

where, λ is the central wavelength, n is the refractive index of the material inside the cavity and L is the cavity length. From Eq. (5), by setting, the cavity length of 8μm, a FSR of 8 μm at central wavelength of 8 μm can be achieved.

The spectral width Δλ of the cavity can be written as:

$$\Delta\lambda = \frac{FSR}{F} = \frac{FSR(1-R)}{\pi R^{1/2}}, \tag{6}$$

where, R is the reflection coefficient. From Eq. (6), to achieve a narrow bandwidth of 20nm, a high reflection of R ~ 0.01 is needed. However, this is hard to obtain using conventional SiN based membranes. To enhance the spectral resolution, a double F-P cavity is design to for a comb filter. Fig. 17 shows the schematic structure of the double cavity comb filter. The two cavities are intentionally designed to be offset for the desired passband. By voltage-tuning the cavity length, the passband can be swiped across the whole LWIR spectrum. We used the transmission matrix to model the performance of the double cavity comb filter. Fig. 18 shows the calculated transmission spectrum of the coupled cavity comb filter. By individually tuning the transmission spectrum of each cavity, a narrow overall passband can be obtained. The passband can be swiped across the whole 8-12 μm band.

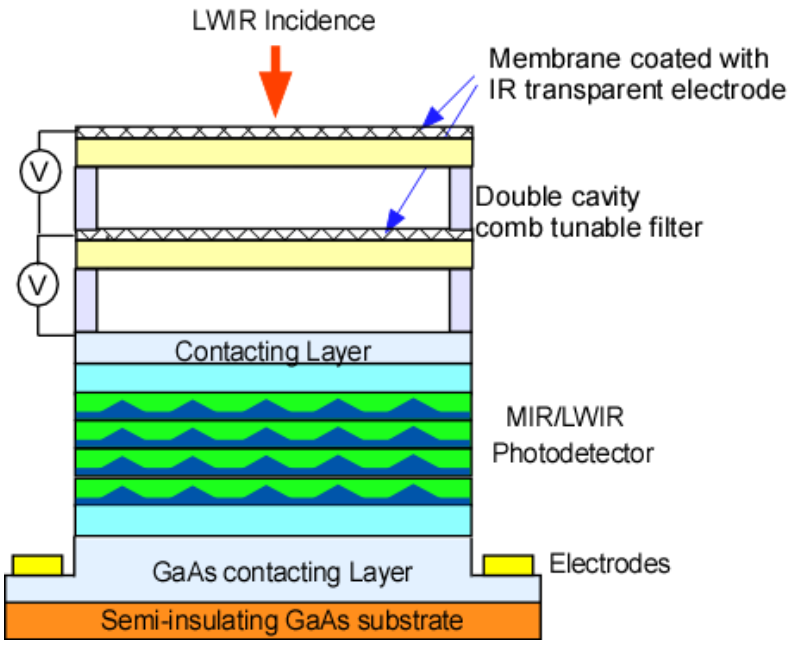

Figure 17, Schematic structure of the double cavity comb filter**.**

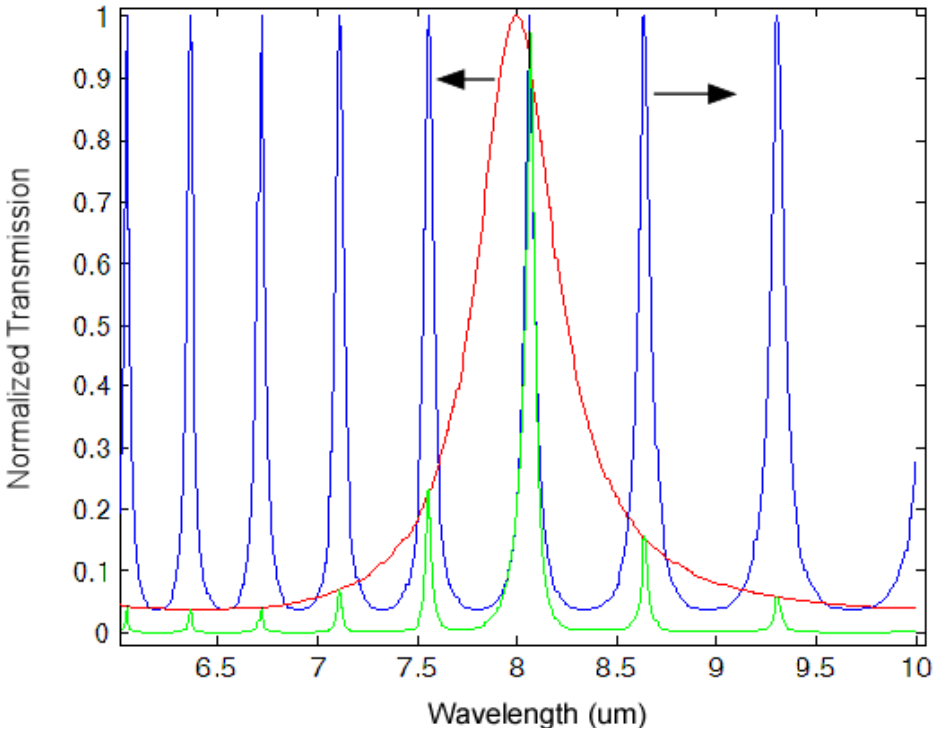

Figure 18, Simulated transmission spectrum of the double cavity comb filter.

2.8 Analyze the linearity of the all-printed transistors

Fig. 19 shows the source-drain I-V characteristics (I_D vs. V_{DS}) of the SWCNT-FET at different gate voltages (V_G) from -2.0V to +2.0V. At a gate bias of 0 V, a turn-on voltage of 1.0 V is observed, indicating Schottky barriers formed between the CNT and the source (S) and

drain (D) electrodes. At the gate biases of 1.0 V and 2.0 V, a larger turn-on voltages of 1.3 V and 1.4 V are measured, respectively. This reflects that the SWCNT band-bending can be tuned by the gate bias, which changes the Schottky barriers and leads to the turn-on voltage variations. At a gate bias of -1.0 V, a nearly linear I-V curve is obtained, indicating the transition from Schottky barrier to Ohmic contact at the SWCNT and the S and D electrode interfaces.

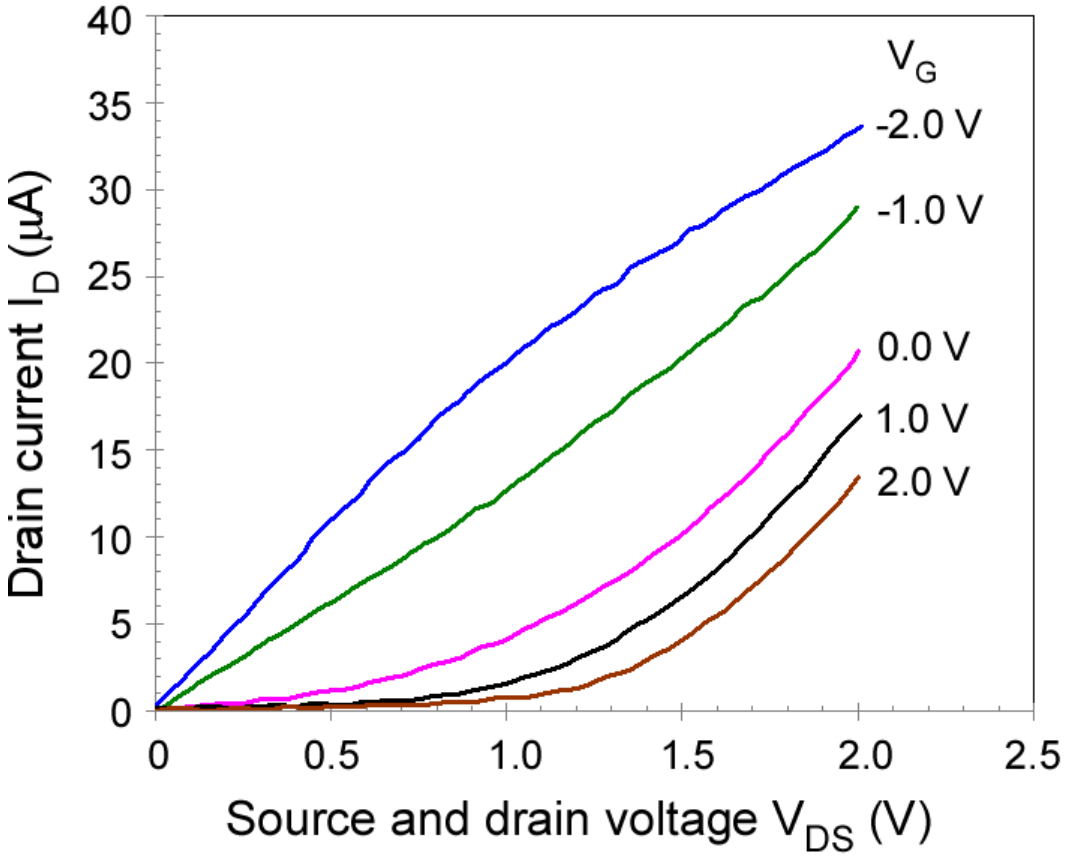

Figure 19, Measured Ids v.s. Vds at different gate voltages.

Fig. 20 show the drain current the I_D v.s. V_G curve at the source-drain voltages V_{DS} of -0.3 V. As the gate voltage V_G increases from -2.0 V to +2.0 V, the drain current voltages I_D decreases from 5.3×10^{-6} (A) to 5.4×10^{-9} (A). If one defines ON and OFF states to be the maximum and minimum steady drain currents I_D, respectively, a high ON/OFF ratio of ~ 10^3 is obtained with a low gate voltage tuning from -2.0 V to +2.0 V.

Since metallic CNTs are conducting materials that are not affected by the gate field effect, the low drain current I_D at the OFF state and the effective gate control of the SWCNT channel indicate that the concentration of the metallic CNT is low in the SWCNT-FET and the SWCNT is primarily semiconducting CNT.

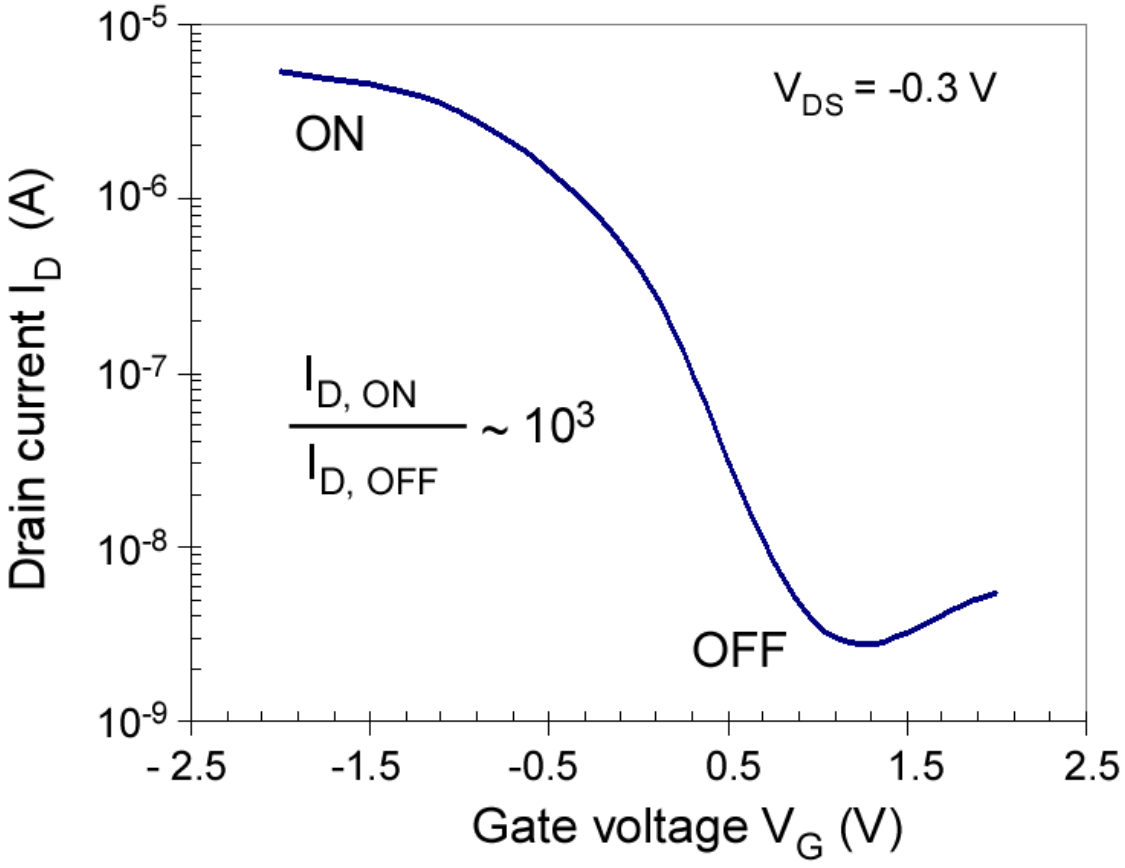

Figure 20. Drain current I_D v.s. V_G curves at the source-drain voltage V_{DS} of -0.3V. A high ON/OFF ratio of ~ 10^3 is obtained.

Fig. 21 shows the logarithmic plots of the I_D v.s. V_G curves in this region. Linear dependence of natural logarithm of the drain current $\ln(I_D)$ on the gate voltage V_G is obtained in this region, indicating exponential dependence of the drain current I_D on the gate voltage V_G. This is similar to a conventional MOSFET in the subthreshold region [12]. The subthreshold slopes are calculated to be 2.1 V/decade, 5.2 V/decade, and 10.3 V/decade at the drain voltages of 1.0 V, 1.5 V, and 2.0 V, respectively. The subthreshold I-V characteristics of an ideal CNT FET can be expressed as [13]:

$$I_D = \frac{4ekT}{h}\exp\left[\frac{e(V_G - V_T)}{kT}\right], \qquad (7)$$

where, e is the charge of an electron, h is the Planck's constant, k is the Boltzmann's constant, and V_T is the threshold voltage. Eq. (1) shows that below threshold the drain current I_D has an exponential dependence on V_G -V_T at a rate of kT/e = 26 mV at room temperature T=300 K. However, the printed SWCNT FET shows a lower exponential dependence rate of 0.9 V, 2.2 V and 4.5 V, at the drain voltages of 1.0 V, 1.5 V, and 2.0 V, respectively. The lower subthreshold slope was also reported [14]. This indicates that the gate bias has a less effective control of the drain current I_D than the ideal CNT FET. The linearity of the all printed flexible SWCNT FET is promising for the flexible phase array antenna application.

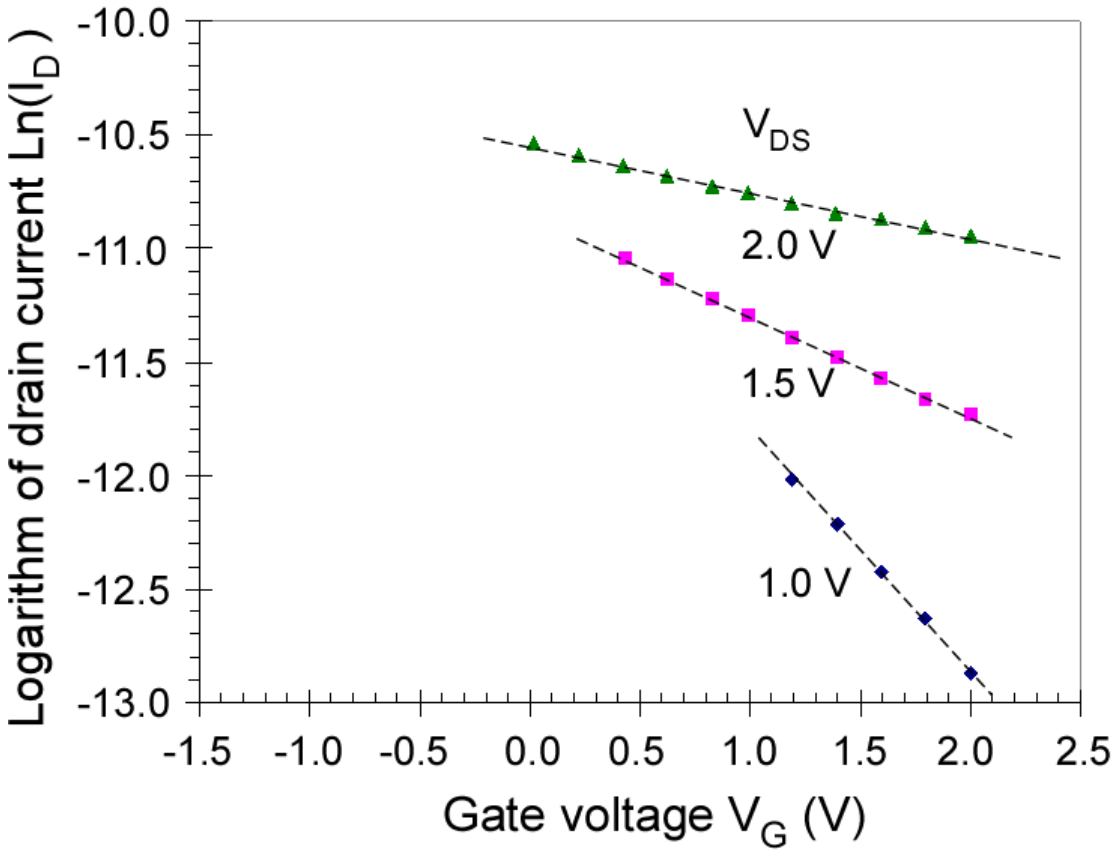

Figure 21. Logarithmic plots of the I_D v.s. V_G curves in the region III of Fig. 20. The dashed lines indicated linear dependence of natural logarithm of the drain current ln(I_D) on the gate voltage V_G.

2.9 Evaluate reliability of the CNT film and develop reliability enhancement techniques

The interfacial stability depends on the strength of the interfacial forces on different surfaces. Most of the interfacial forces are van der Waals interactions, which can be over 10 N/cm^2 in the normal direction and about 8 N/cm^2 in the shear direction [15]. The interfacial adhesion property is characterized by the interfacial work of adhesion using a cantilever test [15]. The schematic of the cantilever test is shown in Fig. 22. The CNT film is deposited on a Si cantilever. The cantilever is then be adhered onto another Si cantilever. The Si cantilever will then be pulled apart from one end in the direction perpendicular to the adhesion plane until it completely separated from the target surface. An optical mini-loading test platform is used to continuously monitor the adhesion force and displacement during this process. To make sure it is quasistatic, the pulling process will be made sufficiently slow. The total adhesion work is the total external work, which can be calculated from the force and displacement integral, i. e.:

$$\phi_{interfacial} = \int F(z)dz\,, \tag{8}$$

Where, *F(z)* is the force applied on the cantilevers, and *dz* is the displacement of the cantilevers.

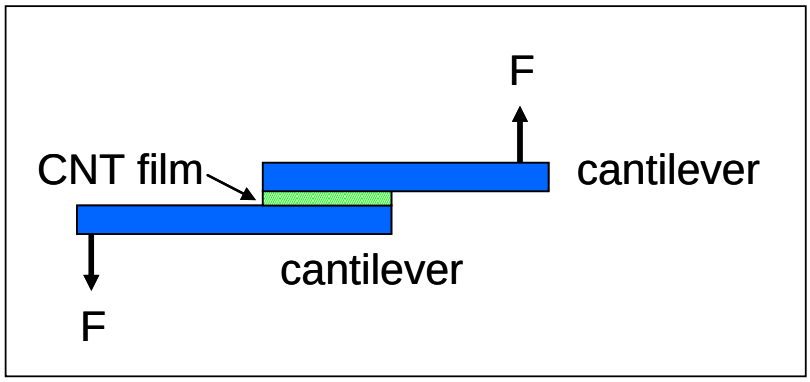

Figure 22, Schematic of the interfacial work of adhesion measurement

Since the interfacial forces are mostly van der Waals interactions, the surface adhesion can be effectively enhanced by strengthen the van der Waals interactions. One way is to introduce interfacial hydrogen by attaching chemical function groups as -OH, -NH_2, and –F to the backbones of the CNT. In this task, we will exam the interfacial work of adhesion on different surfaces and exam the interfacial adhesion work enhancement by introducing different chemical function groups.

Fig. 23 shows the CNT film adhesion with different chemical function groups. The CNT films show excellent adhesion. This can be attributed to the high density CNT networks.

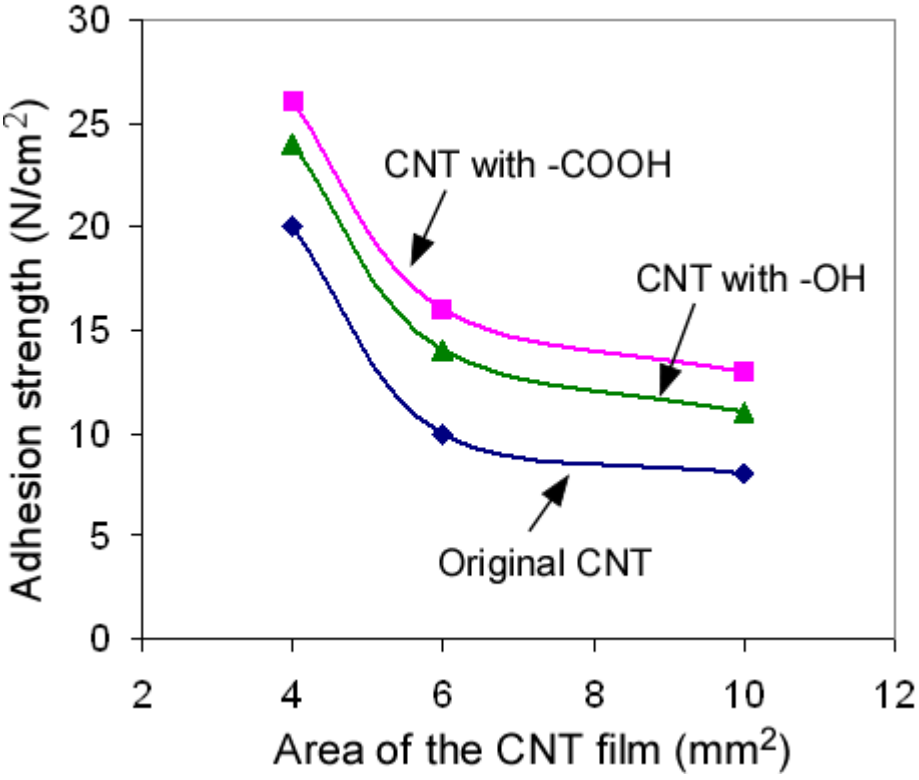

Figure 23. Adhesion the CNT films with different chemical function groups. The CNT films show excellent adhesion. This can be attributed to the high density CNT networks.

Electromigration of atoms happens when atoms are displaced as a result of direct momentum exchange from the moving electrons at the applied electric field. Electromigration is a critical property for many interconnect materials, such as Al, Cu, W, Ag and silicides [18]. Electromigration will cause current-induced mass transport, which when combined with any divergence in mass flux, may cause partial removal of material from one location and buildup of material in other locations. This would result in an open circuit. The higher the current density, the worse the electromigration effect will be.

The electromigration effect for different CNT film thickness and current density levels have been investigated. The CNT circuit properties, including contact resistance, the open circuits rate, didn't change at high and current density levels. This is attributed to the CNT film's ultra-large current carrying capability of ~ 10^6 A/cm^2. This shows that the CNT film are excellent conductive material. The Detailed tests are:

3. PERSONNEL SUPPORTED

- Faculty: Dr. Xuejun Lu, Associate professor, Electrical Engineering
- Graduate students: Guiru Gu
  Runyu Liu
  Yufeng Ling

4. PUBLICATIONS

(1) Jarrod Vaillancourt , Haiyan Zhang , Puminun Vasinajindakaw , Haitao Xia, Xuejun Lu, Xuliang Han , Daniel Janzen , Wu-Sheng Shih , Carissa Jones , Mike Stroder , Maggie (Yihong) Chen , Harish Subbaraman , Ray Chen , Urs Berger , Michael Renn, "All Ink-Jet-Printed Carbon Nanotube (CNT) Thin-Film Transistor on a Polyimide Substrate with an Ultra-high Operating Frequency of over 5 GHz," *Applied Physics Letters*, Vol. 93, No. 24, pp. 243301(2008). **Selected for *Virtual Journal of Nanoscale Science & Technology*.** The Virtual Journal, which is published by the American Institute of Physics and the American Physical Society in cooperation with numerous other societies and publishers, is an edited compilation of links to articles from participating publishers, covering a focused area of frontier research.

(2) Jarrod Vaillancourt, Xuejun Lu, Xuliang Han, Daniel C. Janzen, Wu-Sheng Shih, "High-speed transparent flexible electronics," *Proc. SPIE*, vol. 6940 (2008).

(3) Maggie Yihong Chen, Xuejun Lu, Harish Subbaraman, Ray T. Chen, "Fully printed phased-array antenna for space communications," *Proc. SPIE*, vol. 7318 (2009).

(4) Carissa S. Jones, Xuejun Lu, Mike Renn, Mike Stroder and Wu-Sheng Shih, "Aerosol-jet-printed, high-speed, flexible thin-film transistor made using single-walled carbon nanotube solution," *Microelectronic Engineering* Volume 87, Issue 3, March 2010, Pages 434-437.

(5) All-Printed Linear Flexible Field Effect Transistor based on Purified Single Walled Carbon Nanotubes (SWCNT), Submitted to *Mirco and Nano Letters*, 2011.

(6) Guiru Gu, Puminun Vasinajindakaw, Runyu Liu, Yunfeng Ling, Xuejun Lu, Xuliang Han , Daniel Janzen , Wu-Sheng Shih , Carissa Jones , Mike Stroder , Maggie

(Yihong) Chen , Harish Subbaraman , Ray Chen , Urs Berger , Michael Renn, "All-Printed Thin-film Transistor (TFT) based on Purified Single Walled Carbon Nanotubes (SWCNT) with Linear Response," *Journal of Nanotechnology*, Accepted for publication, 2011.

6. NEW DISCOVERIES, INVENTIONS, OR PATENT DISCLOSURES

None

7. HONORS/AWARDS

IDTechEx, Academic Research and Development Award 2009.

REFEENCES

[1] C. A. Pan and T. P. Ma, "High-Quality Transparent Conductive Indium Oxide Films Prepared by Thermal Evaporation," *Appl. Phys. Lett.*, vol. 37, pp. 163-165 (1980).

[2] Hamberg, A. Hjortsberg, and C. G. Granqvist, "High Quality Transparent Heat Reflector of Reactively Evaporated Indium Tin Oxide," *Appl. Phys. Lett.* 40, 362-364 (1982).

[3] J. P. Zheng and H. S. Kwok, "Low resistivity indium tin oxide films by pulsed laser deposition," *Appl. Phys. Lett.*, vol. 63, pp. 1-3 (1993).

[4] C. G. Granqvist, "Transparent conductive electrodes for electrochromic devices: A review," *Applied Physics A: Materials Science & Processing*, vol. 57, pp. 19-24 (1993).

[5] S. J. Tans, A. R. M. Verschueren, and C. Dekker, "Room temperature transistor based on a single carbon nanotube," *Nature*, vol. 393, pp. 49-52, 1998.

[6] T. Durkop, S. A. Getty, E. Cobas, and M. S. Fuhrer, "Extraordinary mobility in semiconducting carbon nanotubes", *Nano Letters*, vol. 4, pp. 35-39, 2004.

[7] K. Bradley, J. P. Gabriel, and G. Gruner, "Flexible nanotube electronics," *Nano Letters*, vol. 3, pp. 1353-1355, 2003.

[8] E. Artukovic, M. Kaempgen, D. S. Hecht, S. Roth, and G. Gruner, "Transparent and flexible carbon nanotube transistors," *Nano Letters*, vol. 5, pp. 757-760, 2005.

[9] T. Durkop, S. A. Getty, E. Cobas, and M. S. Fuhrer, "Extraordinary mobility in semiconducting carbon nanotubes", *Nano Letters*, vol. 4, pp. 35-39, 2004.

[10] Z. Wu, Z. Chen, X. Du, and J. Logan, "Transparent, Conductive Carbon Nanotube Films," *Science*, vol. 305, pp. 1273 (2004).

[11] M. Kaempgen, G.S. Duesberg, and S. Roth, "Transparent carbon nanotube coating," Applied Surface Science, vol. 252, pp. 425-429 (2005).

[12] S. M. Sze, "Physics of Semiconductor Devices," 3rd Ed. pp. 305, 2007.

[13] J. E. Baumgardner, A. A. Pesetski, J. M. Murduck, J. X. Przybysz, J. D. Adam, and H. Zhang, *Applied Physics Letters*, **91**, pp. 052107, 2007.

[14] S. J. Wind, J.Appenzeller, R.Martel, V.Derycke, and Ph.Avouris, *Applied Physics Letters*, **80**, pp. 3817-3819, 2002.

[15] Y. Zhao, et al, "Interfacial energy and strength of multiwalled-carbon-nanotube-based dry adhesive," J. Vac. Sci. Technol. B, vol. 24, pp. 331-336, 2006.

[16] B. Q. Wei, R. Vajtai, and P. M. Ajayan "Reliability and current carrying capacity of carbon nanotubes," *Appl. Phys. Lett.*, vol. 79, pp. 1172-1174 (2001).